Computers & Geosciences 93 (2016) 103–113

Contents lists available at ScienceDirect

Computers & Geosciences

journal homepage: www.elsevier.com/locate/cageo

Research paper

OpenHVSR: imaging the subsurface 2D/3D elastic properties through multiple HVSR modeling and inversion

S. Bignardi *, A. Mantovani, N. Abu Zeid

University of Ferrara, Via Ludovico Ariosto 35 - 44121, Ferrara, Italy

ARTICLE INFO

Article history:
Received 16 December 2015
Received in revised form
11 April 2016
Accepted 17 May 2016
Available online 19 May 2016

Keywords:
HVSR
Microtremor
Soil amplification
Soil response
2-D
3-D

ABSTRACT

OpenHVSR is a computer program developed in the Matlab environment, designed for the simultaneous modeling and inversion of large Horizontal-to-Vertical Spectral Ratio (HVSR or H/V) datasets in order to construct 2D/3D subsurface models (topography included). The program is designed to provide a high level of interactive experience to the user and still to be of intuitive use. It implements several effective and established tools already present in the code ModelHVSR by Herak (2008), and many novel features such as: -confidence evaluation on lateral heterogeneity -evaluation of frequency dependent single parameter impact on the misfit function -relaxation of V_p/V_s bounds to allow for water table inclusion -a new cost function formulation which include a slope dependent term for fast matching of peaks, which greatly enhances convergence in case of low quality HVSR curves inversion -capability for the user of editing the subsurface model at any time during the inversion and capability to test the changes before acceptance. In what follows, we shall present many features of the program and we shall show its capabilities on both simulated and real data. We aim to supply a powerful tool to the scientific and professional community capable of handling large sets of HSVR curves, to retrieve the most from their microtremor data within a reduced amount of time and allowing the experienced scientist the necessary flexibility to integrate into the model their own geological knowledge of the sites under investigation. This is especially desirable now that microtremor testing has become routinely used. After testing the code over different datasets, both simulated and real, we finally decided to make it available in an open source format. The program is available by contacting the authors.

1. Introduction

Early uses of microtremor for microzonation studies dates back to the 1950s. However, they became increasingly popular in the 90s after the paper of Nakamura (1989), who first introduced the H/V concept (i.e. the ratio between the Fourier spectra of the horizontal and vertical components of the seismic ambient noise). The use of microtremor for the estimation of the local site effects has become increasingly popular especially thanks to its simple approach which only requires the use of a single three-component seismograph and thanks to its applicability which is at present time enhanced by the availability of a wide range of low cost instruments. It is now well understood that the peaks of a HVSR curve occur at the resonance frequencies of the measurement site and are connected to the acoustic impedance contrasts in the subsurface, so that valuable information about the potential seismic amplification at sites where soft sediments resides over bedrock can be achieved by investigating the microtremors. The theoretical basis of the method still remains a matter of discussion. In the early seventies several Japanese scientists (Nogoshi and Igarashi, 1971; Shiono et al., 1979; Kobayashi, 1980) assessed the physical significance of the H/V ratio showing that there is a direct relationship with the ellipticity of Rayleigh waves. Nakamura (1989), on the other hand explained H/V peaks as caused by multiple reflections of vertically incident SH waves. Despite these different explanations, the H/V technique is now widely used for site-specific investigations and microzonation studies (Mucciarelli and Gallipoli, 2001; Scherbaum et al., 2003; Gallipoli et al., 2004a; D'Amico et al., 2008; Albarello et al., 2011). Other applications of the H/V regard the first-order estimation of the geometry of the main seismic reflector and the mapping of the sediments thickness overlying the seismic bedrock (Parolai et al., 2002; Hinzen et al., 2004; D'Amico et al., 2008). Another relevant application of microtremors, regard the identification of the fundamental frequency of buildings and the soil-structure interaction (Mucciarelli and Gallipoli, 2001; Gallipoli et al., 2004b).

* Corresponding author.
E-mail address: sedysen@gmail.com (S. Bignardi).

http://dx.doi.org/10.1016/j.cageo.2016.05.009
0098-3004/

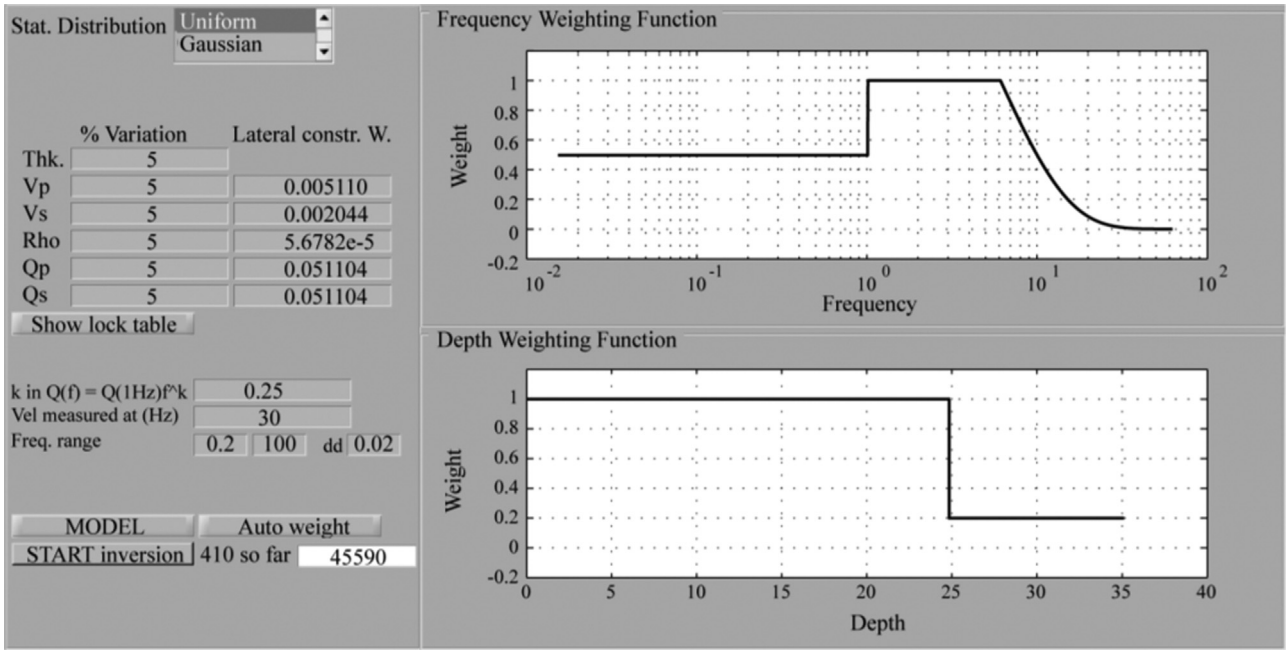

Fig. 1. View of Tab 1: modeling and inversion setup. The controls on the tab allow setting the parameters to simulate the HVSR curves at each location and to setup the inversion.

Originally based on a simple layer over half space subsurface, computational methods for the evaluation of the HVSR curve have recently become available for multi-layer systems where the subsurface is modeled as a stack of infinite homogeneous layers and using different approaches such as computation of mechanical transfer functions (Aki and Richards, 2002; Ben-Menahem and Singh, 1981; Tsai and Housner, 1970) or even exploiting the statistical approach (Sánchez-Sesma et al., 2011; Lunedei and Albarello, 2010, 2015). These modeling strategies have allowed for the investigation of the behavior of a more complex subsurface and have triggered the implementation of codes for the inversion of such curves, as for example the software Grilla (http://www.tromino.eu) or the open source Geopsy (http://geopsy.org). In 2008, Herak published ModelHVSR, a Matlab program capable of obtaining the 1D distribution of the elastic properties of a subsurface by the inversion of a HVSR curve.

After the introduction of this software, HVSR method became so popular and reliable that subsurface investigations based on multiple HVSR measurements performed at different locations started to be used for the construction of 2D subsurface images (Herak et al., 2010). At present time, the strategy behind a 2D HVSR investigation is through "HVSR-profiling", which consists of placing the HVSR curves obtained along a linear profile, back to back and translating the frequency axis into "pseudo-depth" by means of some empirical relation (e.g. $f_0 = V_s/4$ H or using a function where V_s increases with depth), which is usually based on a single and almost arbitrarily chosen average shear waves velocity (V_s) value of the top sediments. The image obtained by HVSR-profiling is only an interpretation of the informative content of the data, but it has proved to be a very useful tool to depict the 2D nature of a subsurface. The final link between this image and the true subsurface is usually provided by comparing the 2D pseudo-profile to the 1D models obtained by inverting the HVSR curves for few key locations.

Despite its usefulness, however, HVSR-profiling does not allow the retrieval of an entire true 2D subsurface profile. This is because only a single value of V_s is used in the frequency-to-depth conversion. Further, to our knowledge, there is no code available, capable of simultaneously inverting multiple HVSR curves, especially when dealing with massive HVSR surveys.

In this paper we introduce an open source program, which we named OpenHVSR, for the simultaneous modeling and/or inversion of massive HVSR datasets. The present program shares some similarities to Herak's ModelHVSR and actually, some of those tools were integrated into the present implementation. This program was especially designed to obtain the 2D and 3D subsurface distribution of the viscoelastic parameters by the inversion of massive HVSR datasets rather than investigating one site at a time. Furthermore, it was designed to give the user the maximum interactivity and dynamicity during the inversion process. Finally, a set of new tools and relevant inversion improvements were implemented.

In what follows, we describe the structure of the program and its capabilities. We shall show an example of inversion of data simulated on a linear array over a subsurface model with lateral variation and finally, we shall illustrate an example of inversion of real data where the depth of the major acoustic impedance contrast (i.e., the so called pseudo-bedrock) was retrieved and where the reconstructed geometry was found in good accordance both with a seismic reflection survey (Fantoni and Franciosi, 2008) running parallel to a portion of our HVSR profile and with other shallow geological information (RER and ENI-AGIP, 1998).

2. Algorithm and optimization strategy

The algorithm is composed of several routines integrated into a main graphical user interface (GUI), which is organized in tabs. The input consists of a text project file which specifies the field geometry (i.e. locations of measurements, including elevation), data path and filenames and one or more files to define an initial subsurface model under the measurement locations. To assure maximum compatibility with commercial acquisition instruments, almost any data file structure is loadable with minimum intervention, provided it is an ASCII format. The subsurface under each measurement site is assumed to be locally layered and the initial subsurface model can be supplied using one or multiple files to

account, if necessary, for different geological situations based on either a geological conceptual model or a proposed hypothesis. The GUI is structured in five tabs, each one devoted to one specific task.

Tab 1 (Fig. 1), is dedicated to the general settings for the simultaneous modeling and/or inversion of a set of HVSR curves. In case of inversion, the input data consists of HVSR curves which are obtained after the elaboration of the corresponding field data by using any third party software (e.g. Grilla, Geopsy, etc.). The forward modeling routine (FWD) implements, in principle, the same modeling strategy present in ModelHVSR (Herak, 2008), but while in ModelHVSR a library compiled for 32 bit computers was provided along with the corresponding mex-fortran source code; here that code was ported to Matlab so that users on 64 bit machines can avoid dealing with mex files compilation and to ensure compatibility with any future release of Matlab. Because of this, one single FWD run is slowed from the 0.002 s of the MEX routine to the 0.01 s for the pure matlab version. The comparison refers to a PC with the following characteristics: INTEL Core 2 CPU 1.8 GHz, 32 bit with 2 Gb RAM, running Windows XP. To the final user the increased computational time does not feel like a burden, especially because of the increased versatility of the interface which makes the experience highly dynamic. However, source files to compile the mex version of the FWD are provided along with the main code to allow users to boost the computation, when desired. The FWD calculates the theoretical transfer function of a layered subsurface based on Tsai and Housner's approach (1970), where the subsurface is represented as a stack of viscoelastic homogeneous layers over a half space and described in terms of thickness (H), density (Rho), compressive and shear wave velocities (V_p, V_s) and corresponding attenuation factors (Q_p, Q_s), which are frequency dependent and follows.

$$Q=Q_0 f^k, \tag{1}$$

where Q_0 is the attenuation factor at 1 Hz and k is a constant which is assumed to be fixed for all sites. Finally, dispersion of body waves is considered through the logarithmic law (Aki and Richards, 2002)

$$v(f)=v\left(f_{ref}\right)\left[1+\left(\pi Q_0\right)^{-1}\ \ln\ \left(f/f_{ref}\right)\right]. \tag{2}$$

For each location, given a local 1-D subsurface, the FWD is used to calculate the amplification spectra of body waves and the body waves-based HVSR curve.

It is worth noting that Tsai and Housner's approach only accounts for the body waves contribution to the HVSR curve, under the assumption of vertical propagation, while in general, both body waves and surface waves contribute to the field data and influence the experimental HVSR (Nakamura, 1996, 2000). Hence, Tsai and Housner's approach will be meaningful as long as the overall response to the incoming wave field (including both body and surface waves) is similar to the one of vertically incident body waves. Of course, this does not means that surface waves can be disregarded, so, for sake of consistency, we provided the capability to simulate the surface waves contribution, which is computed using the modeling routine by Lunedei (2010). We point out that this feature is available for direct modeling purposes and when OpenHVSR is run under the Windows operating system, while the inversion is based on Tsai and Housner's approach only.

The inversion strategy is based on the guided Monte Carlo method (MC), where at every iteration a randomly perturbed version of the best fitting model (i.e. the model which best reproduces the data) is produced and used to compute a set of simulated curves to be compared with the experimental HVSR curves. The generation of many trial models allows exploring the parameters space while looking for a new and better fitting model. The controls placed on this tab allow the user to specify the weights to be associated to different portions of the HVSR curves; choose which material parameters (i.e. the degree of freedom) are randomly perturbed during the inversion process, set which statistical distribution is to be used in perturbing the current model (either uniform or normal) and the maximum amount of the perturbation. Finally, the amount of parameters perturbation can be set as variable with depth. Qualitatively, we can expect different families of parameters (V_p, V_s, H, Q_p, Q_s) to have different impact on the shape of the theoretical HVSR curves. A change in V_p, for example, will have a limited impact when compared to a change in V_s or in thickness, while density variations will have a negligible effect; this however, was discussed by Herak (2008). Further, changes at the deeper layers will mostly affect the low frequency portion of the curves while changes at shallow layers will affect the high frequencies. Since this inversion is focused on retrieving a 2D or 3D subsurface, we need a criterion to decide which set of simulated curves best reproduces the experimental data. This is achieved by calculating the value of an objective function Eq. (3) which is a positive, real value function of the subsurface parameters V_p, V_s, R_o, Q_p, Q_s, and H (called collectively $\boldsymbol{m}$), and seeking its global minimum. Indeed, the objective function can be expressed as

$$E(\boldsymbol{m})=aM(\boldsymbol{m})+bS(\boldsymbol{m})+\sum_{j=1}^{5}\alpha_j R_j(\boldsymbol{m}) \tag{3}$$

where the first term Eq. (4), represents the misfit between the data and the simulated curves,

$$M(\boldsymbol{m})=\sum_{c=1}^{n_c}\left|w_c(f)\left(D_c(f)-D_{0c}(f)\right)\right|^2 \tag{4}$$

the summation on c runs over the n_c sites; $w_c(f)$ is the frequency dependent weighting function and $D_c(f)$, $D_{0c}(f)$ are the simulated and experimental curves respectively. The f stands for frequency and the squared norm is defined as

$$|F(f)|^2=\int_{f_{min}}^{f_{max}} F^2(f)\,df \tag{5}$$

The term in Eq. (4) alone represents the classic objective function as it is usually encountered in the literature on the topic. The second term Eq. (6),

$$S(\boldsymbol{m})=\sum_{c=1}^{nc}\left|w_c(f)\left(\frac{\partial D_c(f)}{\partial f}-\frac{\partial D_{0c}(f)}{\partial f}\right)\right|^2 \tag{6}$$

introduces a novel forcing condition on the slope of the curves. Indeed, the main information of an HVSR curve is represented by the peaks location. Of course, the width of the peaks and their amplitude brings valuable information about the subsurface impedance contrasts; but while the location of the peaks is clearly identifiable in the experimental data, their width and relative amplitude can vary depending on many factors such as for example the energetic content of the recorded signals or even the coupling between the soil and receiver. So while the term in Eq. (4) forces the synthetics to match the experimental curve amplitude, the term in Eq. (6), by forcing the slope difference of experimental and synthetic curves to be minimum, it is more suitable for constraining the peak locations even when amplitudes poorly match. The introduction of this term represents a simple yet crucial improvement when attempting the inversion of low quality curves. Constants a and b in Eq. (3) balance the relative weight of the $M(\boldsymbol{m})$ and $S(\boldsymbol{m})$ terms and are usually chosen by the user because they may change depending on

the quality of the investigated data. Here we used $a=0.9$ and $b=0.1$, but we found it beneficial to use $a=0.6$ and $b=0.4$ for very low quality curves. From now on, we will refer to misfit as the sum of the first two terms in Eq. (3). Finally the third one is a regularizing term Eq. (7),

$$R_j(\boldsymbol{m}) = \sum_{k,l=1}^{n_c} B_{kl} \int_{Z_{min}}^{Z_{max}} \left(m_j^k(z) - m_j^l(z)\right)^2 dz \tag{7}$$

which, for each value of the index j, implements a smooth lateral variation constraint on a particular parameters subset $m_j = V_p$, V_s, R_o, Q_p, Q_s, for $j=1$–5 respectively. Each pair k, l in the summation is used to select the subsurface models at two different locations and the integral over z will take its minimum value when the parameter set being considered shows no lateral variation. Finally, B_{kl} can take values between 0 and 1 depending on the relative distance among the two locations and has the effect of relaxing the lateral constraint with the distance. If set to zero, the subsurface model under kth and 1th locations are uncoupled and the smooth lateral variation constraint is not enforced between these sites. The parameters α_j in Eq. (3) highlight the importance of the regularizing term for the different subsets of parameters and are usually chosen by the user, even though an automatic selection strategy is also available. Of course in the frame of MC there is no numerical instability so that the regularizer has only the purpose of smoothing the model and can be excluded if desired. It must be mentioned that assuming a local 1-D subsurface under each site is implicitly equivalent to assume that structure of ambient vibrations at nearby sites is negligibly affected by the presence of lateral variations. This, of course, is only a convenient approximation which is best realized when the size of lateral variations is much larger than the wavelength of seismic waves responsible for the observed HVSR.

Proceeding further, Tab 2, (Fig. 2) is devoted to the independent optimization of the local 1D subsurface at the site of the specific HVSR curve at hand. Tab 2 shows: an aerial view of all measurement locations where the currently selected site is highlighted, the subsurface parameters organized as a table, the 1D profile of one selectable media property, and the HVSR curve plot along with error bars (if available). Finally, the simulated response of the supplied and/or the best model are shown for comparison with the data. When inversion is running, all tables and graphs are dynamically updated to allow the user to visually inspect the inversion process. Further, the progress of minimization is shown in the misfit-vs-number of iterations plot. The inversion can be paused at any time and when stopped, the user is allowed to inspect the 1D graph window where the fifty most fitting models are shown along with the best match. Furthermore, the experienced user is also allowed to manually correct the subsurface model both on the basis of their own knowledge about the local geology, or alternatively after using the tools of Tabs 4 and 5 (discussed later). The effect of the correction can be tested prior to deciding whether to keep or discard the introduced changes. Finally, when for a given location a satisfactory fit is reached, the user is also allowed to extend the local subsurface model to the previous/successive location or even to the entire survey. A specific local model, once optimized can also be locked in order to prevent further modifications or in order to introduce an abrupt discontinuity when it is known to exist.

Tab 3, (Fig. 3) is a 2D/3D view of the best fitting subsurface, while.

Tab 4 (Fig. 4) allows for plotting the confidence in the result with respect to two chosen degrees of freedom (d.o.f) by using the "CONF_LIM" routine (Herak, 2008) which, in turn, is based on the F-distribution computation (Mayeda et al., 1992; Bianco et al., 2002). When the misfit is plotted against two d.o.f. pertaining to the same site, the meaning of the figure is exactly the same of Herak's. The consistent improvement is that now the confidence plot can be expressed as a function of d.o.f. pertaining to different sites thus allowing the evaluation of the confidence regarding any found lateral heterogeneity.

Finally, Tab 5 (Fig. 5) implements a novel strategy to investigate the confidence in any specific model parameter. It allows for plotting the variation of the contribution to the misfit associated to the curve recorded at a specific location c, with respect to a chosen

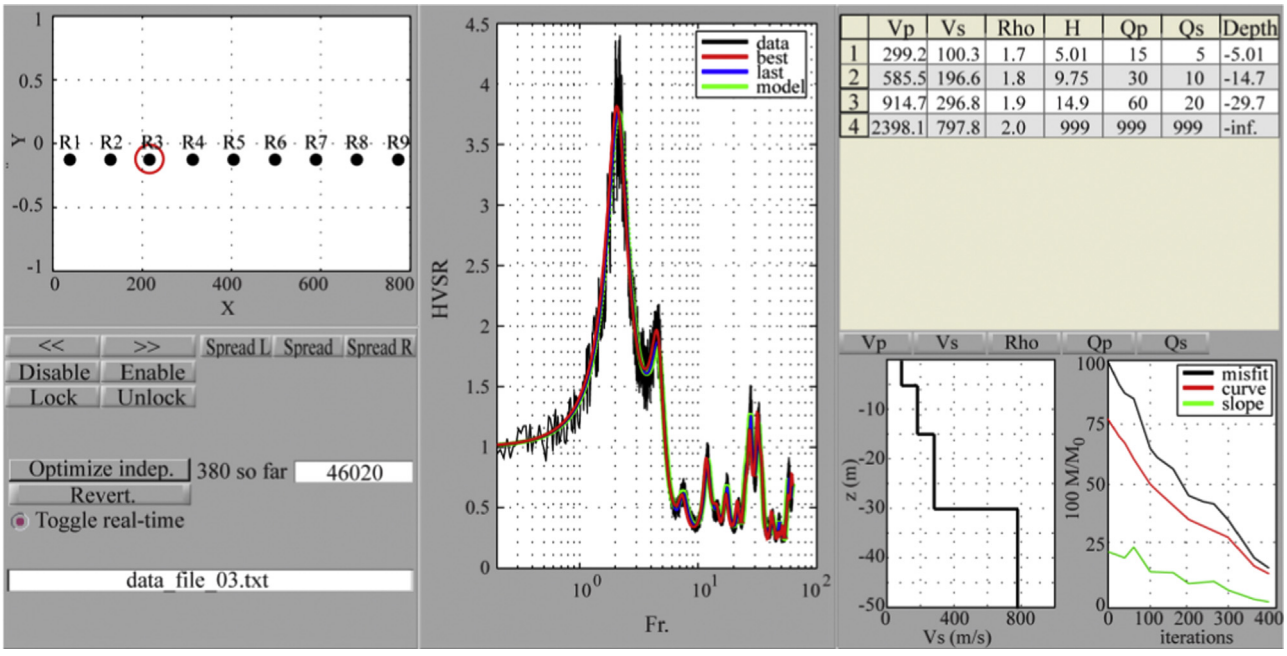

Fig. 2. View of Tab 2, single curve optimization. Panel on the left shows an aerial view of the measurement locations, the selected data and inversion controls. Central panel shows the experimental HVSR compared to the simulated curves. On the right panel, the subsurface parameters and the evolution of the inversion process are shown.

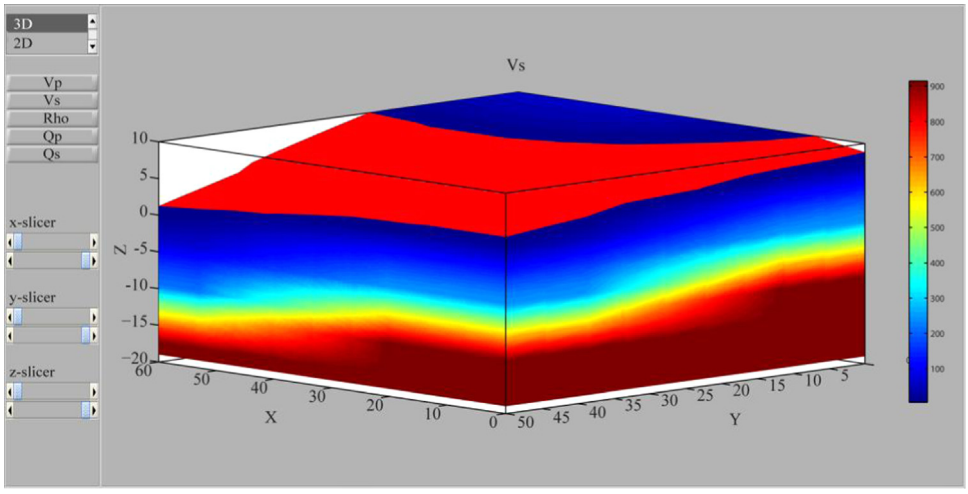

Fig. 3. Tab 3; it allows to inspect the 2D/3D subsurface model.

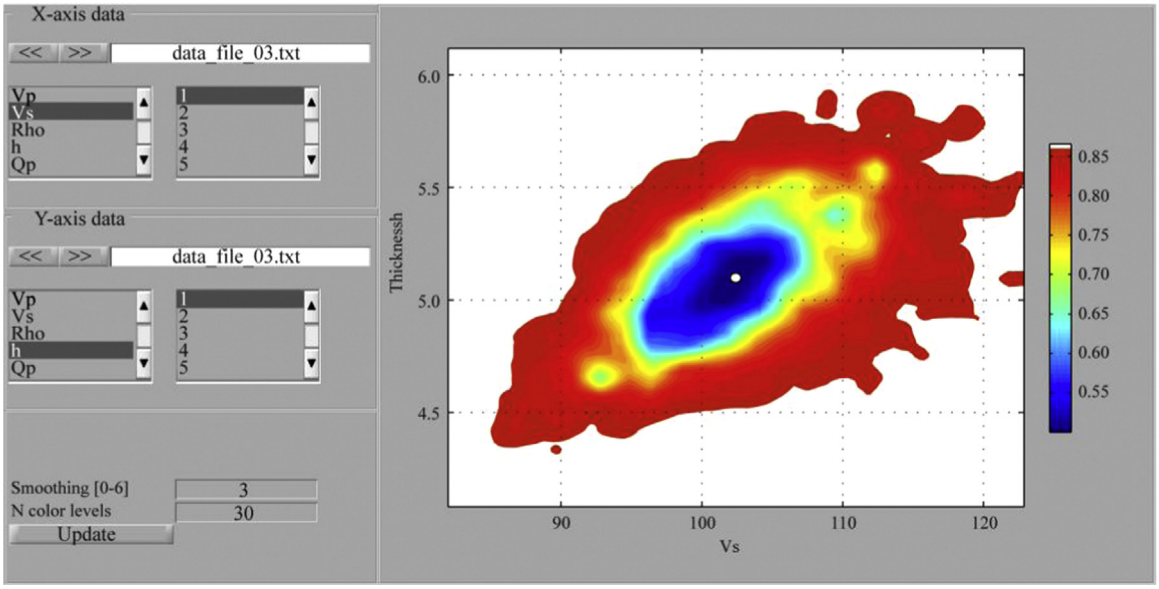

Fig. 4. Tab 4 shows the confidence of the best model as a function of two selected parameters. When the two parameters pertain to different measurement locations, it can be used to gain confidence on lateral variations.

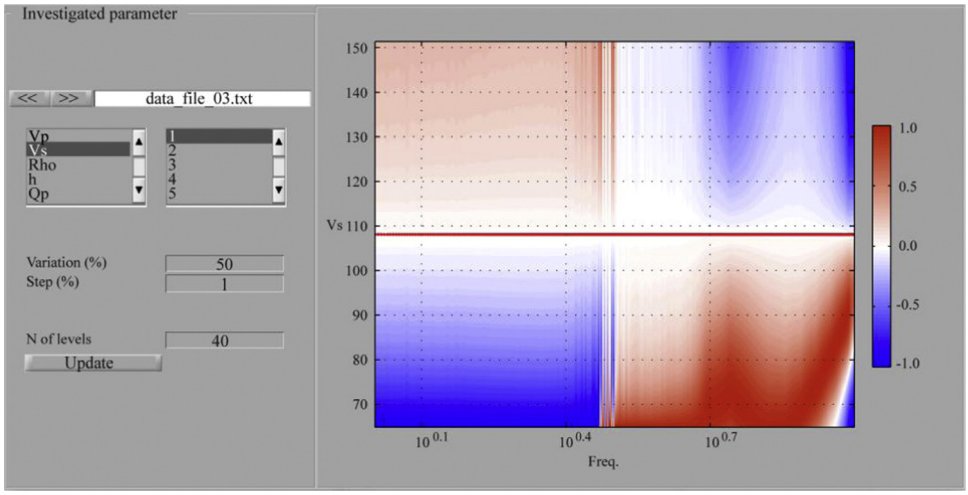

Fig. 5. Tab 5, "Single parameter sensitivity", i.e. the variation of dE (Eq. (8)) with respect to a single parameter.(For interpretation of the references to color in this figure, the reader is referred to the web version of this article.)

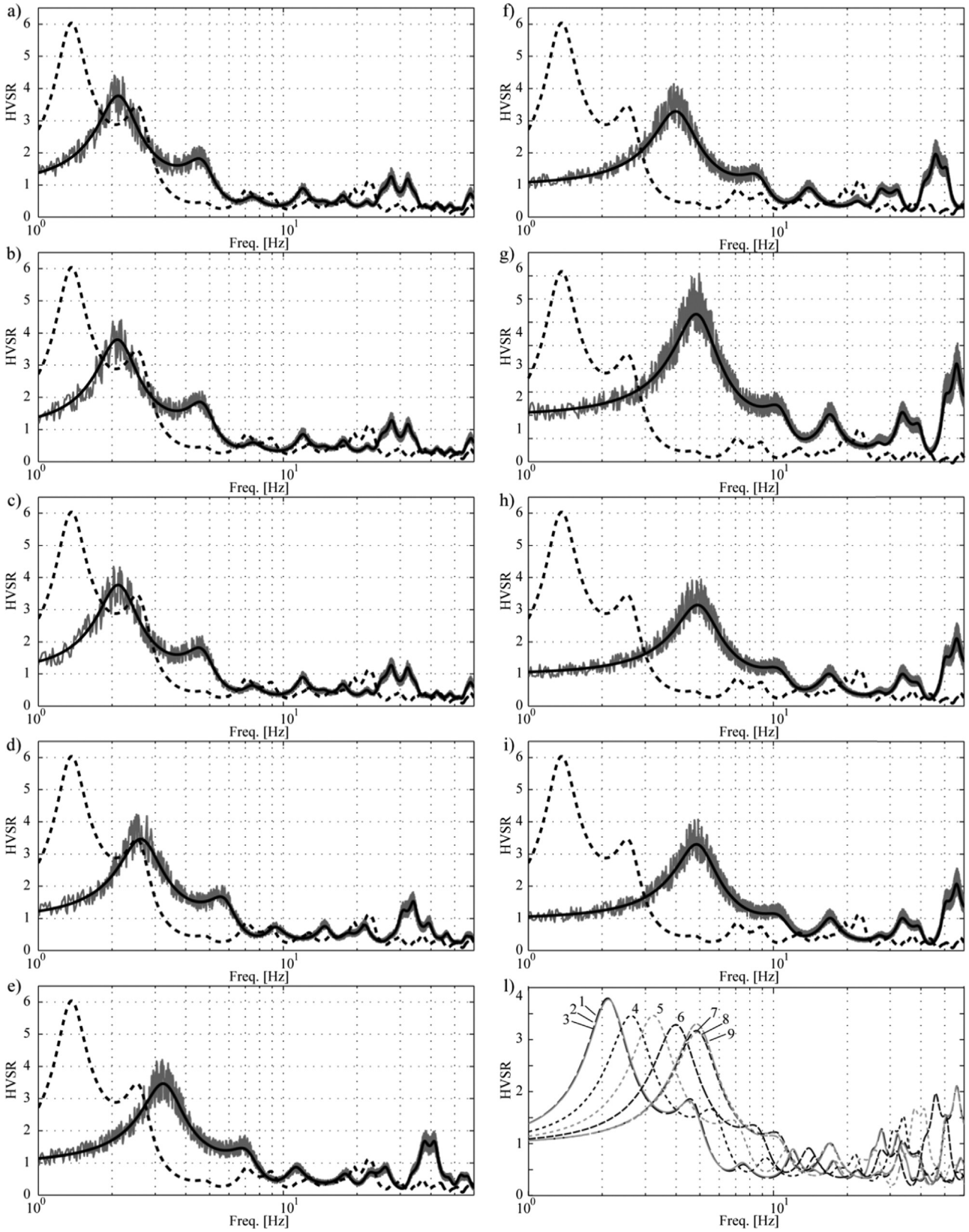

Fig. 6. Curve fitting is shown in figures a–i for the nine receivers, R1–R9, of a simulated linear array ideally placed on top of the model of Fig. 7a, b. The gray line is the simulated data curve contaminated with 15% random Gaussian noise. The black curve is the result of inversion while the dashed one is the starting model response. Inverted HVSR curves are also shown in Fig. 1, to highlight the effect of the sloping section of the profile to the principal peak. Curves are numbered as the receivers, where R1 is the leftmost one.

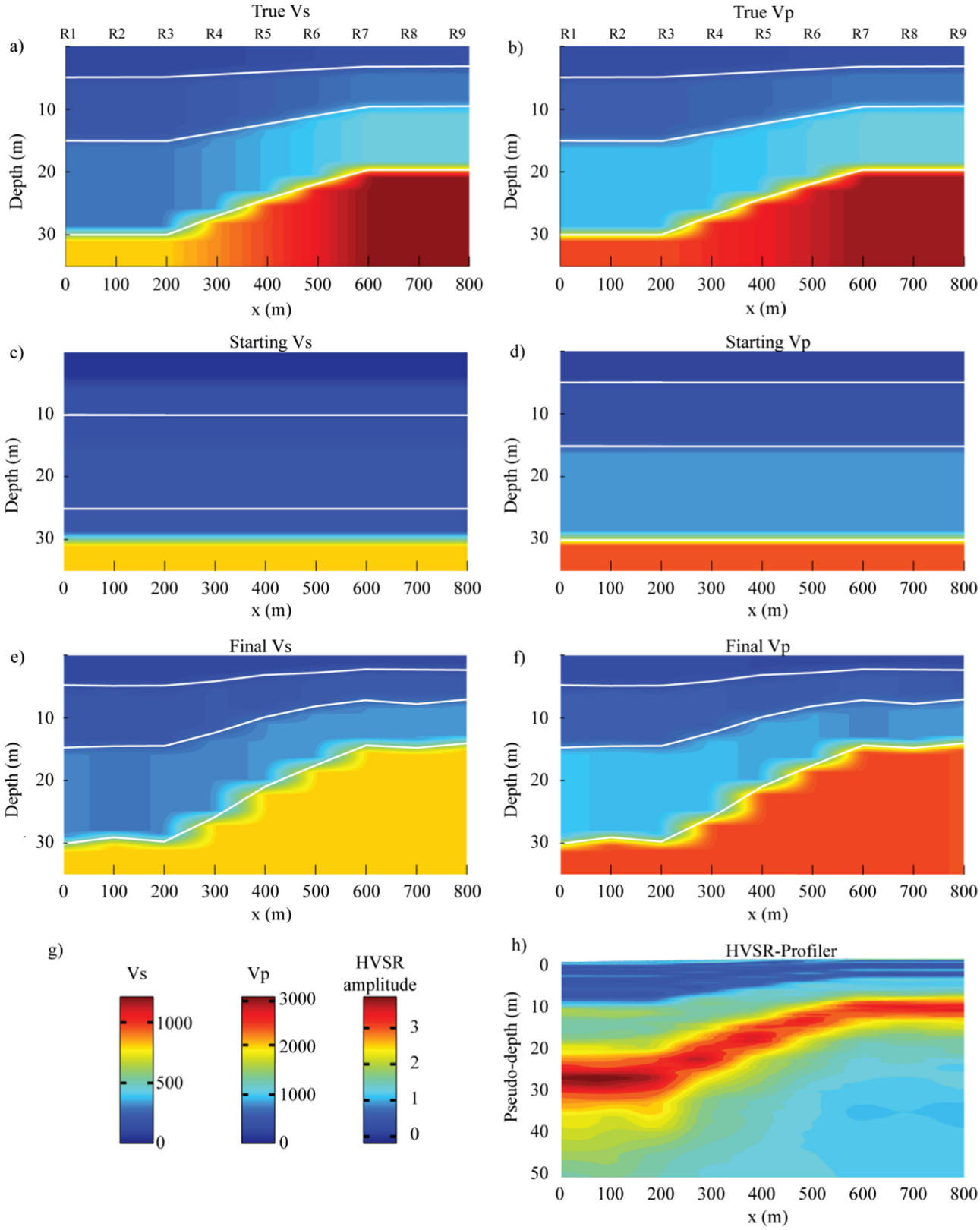

Fig. 7. Example of inversion result. True V_s and V_p profiles are shown in figures a and b respectively. The values under receivers R1–R3, correspond to the example model in Herak 2008. V_s and V_p starting models used in inversion are shown in figures c and d respectively, while the corresponding retrieved profiles are shown in e and f. Figure g shows the color scales used in these images, while figure h shows the "HVSR-profiling" of the same data obtained by placing the HVSR curves back to back and translating the frequency axis into "pseudo-depth" by assuming the average velocity of the soft layers stack as $V_s = 230$ m/s. (For interpretation of the references to color in this figure legend, the reader is referred to the web version of this article.)

parameter m, Eq. (8) before the integration with respect to frequency of Eq. (5)

$$dE_{(c,f,\boldsymbol{m})}=a\left[\left[\left(D_{c\,(f,\boldsymbol{m})}-D_{0c}\right)^2-\left(D_{(c,f,\boldsymbol{m}_{best})}-D_{0c}\right)^2\right]\right]+ b\left[\left[\left(\frac{\partial D_{c\,(f,\boldsymbol{m})}}{\partial f}-\frac{\partial D_{0c}}{\partial f}\right)^2-\left(\frac{\partial D_{c\,(f,\boldsymbol{m})}}{\partial f}-\frac{\partial D_{0c}}{\partial f}\right)^2\right]\right] \quad (8)$$

As stated previously, when a limited portion of the HVSR curve is inverted, the subsurface elastic parameters are randomly perturbed. When a good match between the data and the simulated curve is found, the subsurface model that produced the simulated curve is accepted. Unfortunately, if some parameter has a poor influence on the shape of the simulated curve and in turn on the misfit (i.e. has a low sensitivity), a good match can be found even if an improbable value of such a parameter is present. The function dE(f,$\boldsymbol{m}$), allows the user to judge which portion of the HVSR curve is affected by a change in a specific parameter. Further, positive and negative variations of dE(f,$\boldsymbol{m}$), plotted in red and blue respectively, are associated with an increase and decrease of the frequency dependent contribution to the misfit. By this test, we can judge how a particular parameter impacts the misfit value, which portion of the HVSR curve is accountable for the change and how that parameter should be changed in order to decrease the misfit. Furthermore, when unreasonable parameter values are present, it can guide the user to find the correction to obtain a more plausible model.

3. Simulated data example

We firstly tested the algorithm on simulated data. To do so, we generated nine different HVSR curves along a profile starting from location R1 ($x=0$) to location R9 ($x=900$) m and spaced at 100 m intervals (Fig. 7). The obtained curves were perturbed with a normally distributed random noise with one sigma corresponding to 15% of perturbation. The noisy curves (a)–(i) in Fig. 6 were then used as input data for the inversion.

In 2010, Herak showed a successful inversion performed by optimizing V_s and V_p of the layers while keeping all other parameters fixed. In this test, we relaxed these constraints allowing for both velocities (V_s, V_p) and thicknesses (H) to change. The half-space parameters were kept fixed, however, this constrain is known to have a negligible impact on the inversion. In order to obtain a rough starting model for the laterally constrained optimization, we independently optimized the subsurface model under each HVSR curve by allowing a 5% perturbation for the first 3000 iterations and then successively allowing 15% perturbation for the next 5000 iterations. In general, a few hundred generations per location was sufficient to find the best 1D local model; but we decided to extend the computation up to 8000 random generations to enhance the sampling of the parameter space.

Correspondingly, the true subsurface model is plotted in terms of 2D profiles of Vp and V_s in Fig. 7a and b respectively. The subsurface under stations R1–R3 is assumed to be the same used by Herak (2008). The thickness regularly decreases between stations R3 and R7 and then becomes constant under locations R7–R9. Finally, the inversion was performed by starting from the model in Fig. 7c and d. Later, in order to obtain the model which best satisfies Eq. (3), we started from the latter rough model, composed of all the optimal 1D local models and we performed 30,000 perturbations of the entire profile as a whole, allowing perturbations of 20% with respect to the best model. The results in the data space are shown in Fig. 6a–i, where the best fitting curves (solid black) are compared to the data (solid gray) and to the initial model response (dashed black). Fig. 6l shows the best curves obtained at different locations. The best result in the parameter space is shown in term of V_s and V_p profiles (Fig. 7e, f). Further, for sake of comparison, the result of HVSR-profiling, where the HVSR amplitude is plotted in terms of pseudo-depth is shown in Fig. 7h. To obtain the latter figure we used, for the frequency-to-depth conversion, $V_s=230$ m/s which in this case proved to be the correct value. It can be noted that the profiler result is in good accordance with the inversion.

4. Real data case

In this section we present a simplified inversion example of multiple HVSR curves collected along a linear profile in the framework of the Italian DPC-INGV Seismological Projects S1 (Abu-Zeid et al., 2014; Mantovani et al., 2015) with the purpose of acquiring the deep shear wave velocity (up to 150 m depth) in the Province of Ferrara, both for microzonation purposes and to document the occurrence of recent tectonic evolution of the central-eastern sector of the Po Plain nearby the town. A geophysical survey along two profiles was carried out, ca. 27 km-long almost perpendicular to the regional trend of the underlying tectonic structures (Fig. 8a, b), based essentially on passive seismic measurements.

The measurements were performed using a three-component short-period seismometer ($f_c=2$ Hz) for time intervals of 50 min and HVSR curves were computed using a window size of 60 s.

In Fig. 9 we present a portion of the 2D V_s profile obtained after inverting the subset of the data highlighted with the green squares in Fig. 8. Along the investigated area, the pseudo-bedrock (white dashed line in Fig. 9a) undergoes various depth variations and it is expected to gently deepen moving from the south to the north (R1–R8 in Fig. 9a). The main frequency peak observed in the Po Plain is well documented to be variable depending on the location (Martelli et al., 2014; Paolucci et al., 2015) with fundamental frequency ranging from 0.5 to 1.5 Hz. Considered this, the analysis was limited in the frequency band between 0.5 and 6 Hz. The obtained depth of the major impedance contrast is consistent with those of the other geophysical tests and available information about the subsurface stratigraphy. In particular, the pseudo-bedrock here detected could correspond to the contact between two sedimentary cycles, both belonging to an higher rank sedimentary cycle represented by the Upper Emiliano-Romagnolo Synthem (RER and ENI-AGIP, 1998).

In the following, Fig. 9a shows the V_s profile obtained by OpenHVSR and for sake of comparison Fig. 9b shows the corresponding HVSR-profiling. Further, Fig. 10a–h, show the comparison between the data and the theoretical curves in the frequency band 0.5–6.0 Hz. Such a result was achieved using a semi-automatic strategy. We performed three sessions of model improvement, each consisting of separately inverting each curve by allowing a 5% perturbation in the Monte Carlo algorithm and running 5000 single-curve random perturbations, followed by 10,000 laterally constrained perturbations. We started from a simple 4 layers model and whenever necessary, we progressively increased the number of layers among sessions. This was possible thanks to the improved flexibility of the interface which allowed to test the changes introduced by adding new layers, and allowed to quickly save and reload the models obtained after each modification. A fourth and final session was performed after the subsurface model was considered satisfactory; we increased the amount of perturbation up to 20%, allowing 10,000 single-curve perturbations, followed by 10,000 laterally constrained perturbations. The whole process required roughly 3 h on an INTEL I7 (1.8–2.4 GHz), 8 Gb RAM computer running Linux.

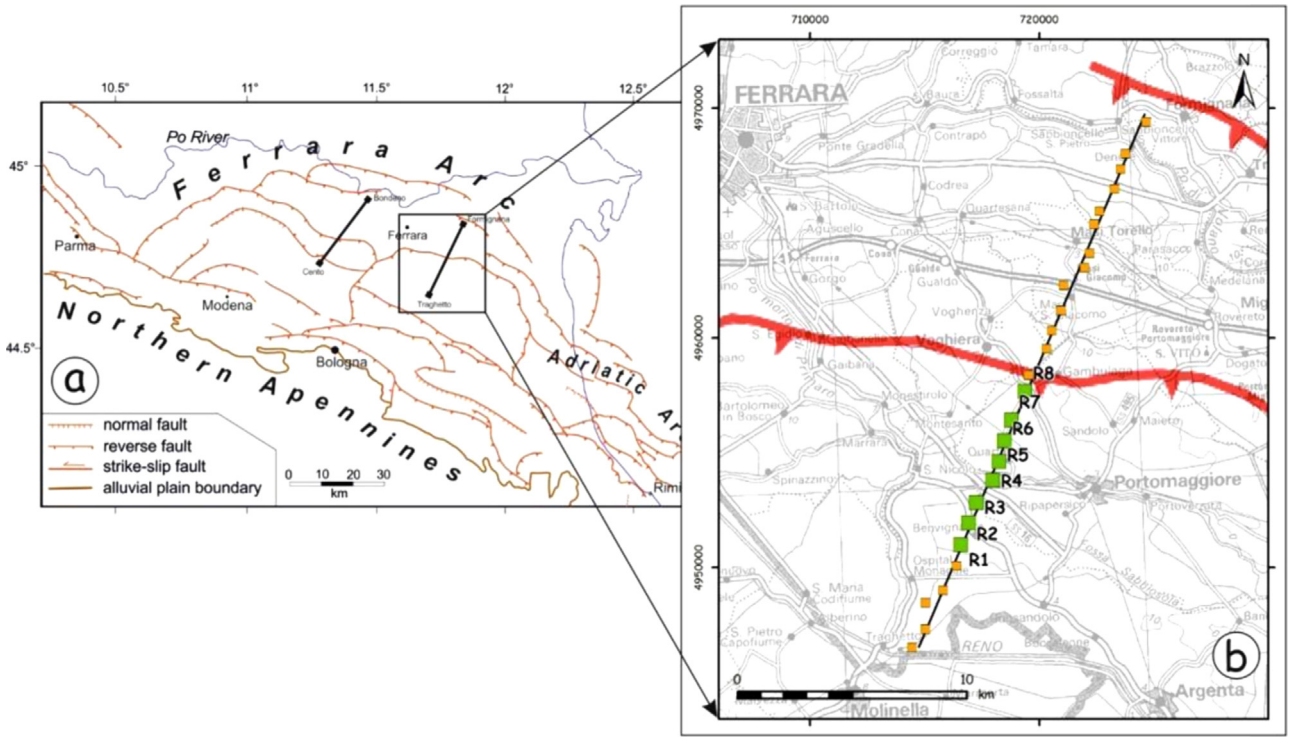

Fig. 8. (a) Simplified tectonic map of the blind northern Apennines showing the two studied profiles (Pieri and Groppi, 1981). (b) Location of the single-station measurements (squares). HVSR measurements used in the example are highlighted in green. (For interpretation of the references to color in this figure legend, the reader is referred to the web version of this article.)

5. Conclusions

In this paper, we introduced a novel program developed in the Matlab environment for the simulation and/or inversion of massive HVSR datasets with the goal of constructing a 2D/3D subsurface in terms of viscoelastic parameters; which to our knowledge has no analogue in the literature. The program was designed for maximum interactivity and dynamicity. The underlying forward routine, available in Fortran from Herak (2008) was ported into Matlab for compatibility with future releases of this platform. The inversion algorithm, based on the guided Monte Carlo method, is fully customizable and it implements many novel features not seen previously. In particular the subsurface model perturbation can be set to be depth dependent, relaxation on elastic parameter constraints now allows the user to account for the water table and finally, the user can, at any time, pause the inversion and manually investigate or modify the subsurface model parameters with the capability of testing the result of such a change before accepting it. Other than the confidence estimation tools already present in ModelHVSR which were integrated in the present code and are now extended to the lateral variation confidence evaluation, a novel tool was introduced which allows the user to investigate how each parameter perturbation impacts different portions of the HVSR curve. Furthermore, two novel terms were introduced in the objective function of the inversion algorithm. The first is based on matching the slope of the HVSR

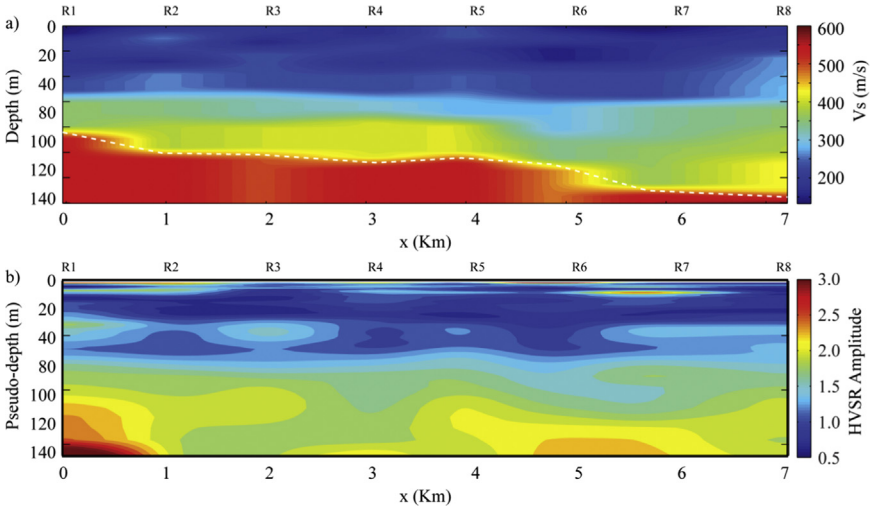

Fig. 9. Results for the real data case, 8 HVSR curves performed along a profile running ESE to the city of Ferrara, Italy; (a) The 2-D V_s profile obtained by the inversion shows the seismic pseudo-bedrock to steeping toward NNE. (b) For sake of comparison, the corresponding image obtained by HVSR-profiling, which consists of placing the HVSR curves back to back and translating the frequency axis into "pseudo-depth" by assuming, for the soft layers $V_s = 350$ m/s.

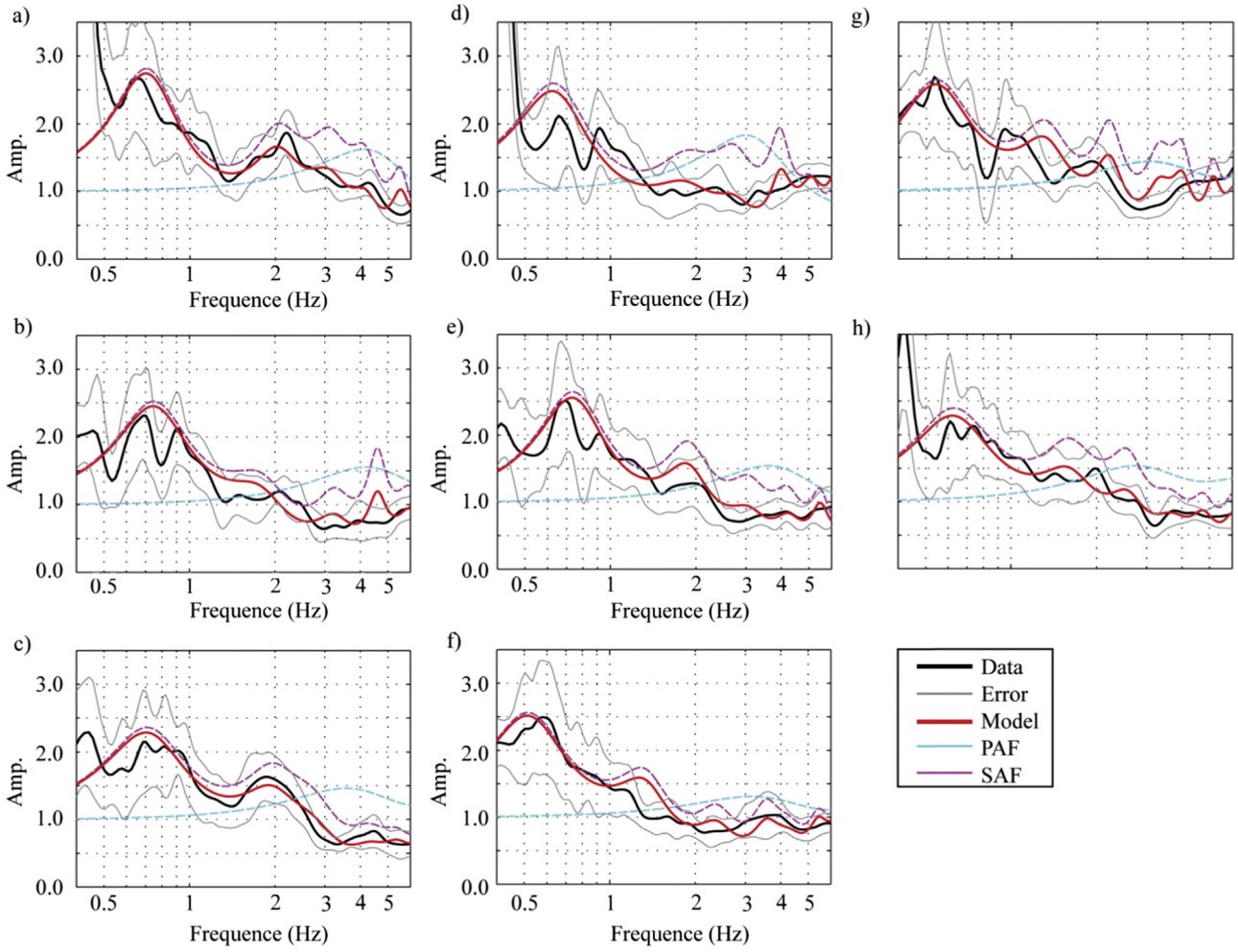

Fig. 10. Results of the inversion in the data space; (a)–(h) shows the best match we achieved for the frequency band 0.5–6.0 Hz, corresponding locations over the profile are indicated in Fig. 8 with R1–R8 labels respectively. HVSR's and error bounds are drawn in black and gray respectively, while the best model response is drawn in red. Further, amplification functions for P (PAF) and S (SAF) waves are drawn in cyan and magenta respectively. (For interpretation of the references to color in this figure legend, the reader is referred to the web version of this article.)

curves rather than their amplitudes and allows for better constraining of the peaks position, especially when inverting low quality curves. The second term is a regularizing term which can be used to impose a lateral smoothness condition. Effectiveness of the method was successfully shown both on simulated and real data. The successful results encouraged and motivated us to publish the present code in an open source format.

Acknowledgments

The authors would like to thank the University of Ferrara for sponsoring this research and in particular Prof. Giovanni Santarato, University of Ferrara, for the valuable advice regarding the mathematical implementation and the optimization of the graphical interface and Prof. Anthony Yezzi (Georgia Institute of Technology) for the valuable suggestions during the development of this work. We would like to thank the Lions Club International - District 108 Tb, Bologna (Italy) for the support in acquiring of the instrumentation. Finally, we would like to thank Prof. Marijan Herak (University of Zagreb, Croatia), who first developed and distributed ModelHVSR as open source, making an implementation base available for some of the tools integrated into this code.

Appendix A. Supplementary material

Supplementary data associated with this article can be found in the online version at http://dx.doi.org/10.1016/j.cageo.2016.05.009.

References

Abu-Zeid, N., Bignardi, S., Caputo, R., Mantovani, A., Tarabusi, G., Santarato, G., 2014. Shear-wave velocity profiles across the Ferrara arc: a contribution for assessing the recent activity of blind tectonic structures. In: Proceedings of the 33th GNGTS National Convention, vol. 1, pp. 117–122.

Aki, K., Richards, P.G., 2002. Quantitative Seismology, second ed., University Science Books, Sausalito, CA, p. 700.

Albarello, D., Cesi, C., Eulilli, V., Lunedei, E., Paolucci, E., Pileggi., D., Puzzilli, L.M., 2011. The contribution of the ambient vibration prospecting in seismic microzoning: an example from the area damaged by the 26th April 2009 l'Aquila (Italy) earthquake. Boll. di. Geofis. Teor. Ed. Appl. 52 (3), 513–538.

Ben-Menahem, A., Singh, S.J., 1981. Seismic Waves and Sources. Springer-Verlag, New York.

Bianco, F., Del Pezzo, E., Castellano, M., Ibanez, J., Di Luccio, F., 2002. Separation of intrinsic and scattering seismic attenuation in the southern Apennine zone, Italy. Geophys. J. Int. 150, 10–22.

D'Amico, V., Picozzi, M., Baliva, F., Albarello, D., 2008. Ambient noise measurements for preliminary site-effects characterization in the urban area of Florence, Italy. Bull. Seismol. Soc. Am. 98, 1373–1388.

Fantoni, R., Franciosi, R., 2008. Geological sections crossing Po Plain and Adriatic foreland. Rend. Online Soc. Geol. Ital. 3 (1), 367–368.

Gallipoli, M.R., Mucciarelli, M., Eeri, M., Gallicchio, S., Tropeano, M., Lizza, C., 2004a. Horizontal to Vertical Spectral Ratio (HVSR) measurements in the area

damaged by the 2002 Molise, Italy earthquake. Earthq. Spectra 20 (1), 81–93.
Gallipoli, M.R., Mucciarelli, M., Castro, R.R., Mochavesi, G., Contri, P., 2004b. Structure, soil-structure response and effects of damage based on observations of horizontal-to-vertical spectral ratios of microtremors. Soil Dyn. Earthq. Eng. 24, 487–495.
Herak, M., 2008. ModelHVSR-A Matlab tool to model horizontal-to-vertical spectral ratio of ambient noise. Comput. Geosci. 34, 1514–1526.
Herak, M., Allegretti, I., Herak, D., Kuk, K., Kuk, V., Marić, K., Markušić, S., Stipčević, J., 2010. HVSR of ambient noise in Ston (Croatia): comparison with theoretical spectra and with the damage distribution after the 1996 Ston-Slano earthquake. Bull. Earthq. Eng. 8, 483–499.
Hinzen, K.G., Scherbaum, F., Weber, B., 2004. On the resolution of H/V measurements to determine sediment thickness, a case study across a normal fault in the Lower Rhine embayment, Germany. J. Earthq. Eng. 8, 909–926.
Kobayashi, K., 1980. A method for presuming deep ground soil structures by means of longer period microtremors. In: Proceedings of the 7th WCEE, September 8–13, Istanbul, Turkey, vol. 1, pp. 237–240.
Lunedei, E., Albarello, D., 2015. Horizontal-to-vertical spectral ratios from a full-wavefield model of ambient vibrations generated by a distribution of spatially correlated surface sources. Geophys. J. Int. 201 (2), 1140–1153. http://dx.doi.org/10.1093/gji/ggv046.
Lunedei, E., Albarello, D., 2010. Theoretical HVSR curves from full wavefield modelling of ambient vibrations in a weakly dissipative layered Earth. Geophys. J. Int. 181, 1093–1108. http://dx.doi.org/10.1111/j.1365-246X.2010.04560.x.
Mantovani, A., Abu-Zeid, N., Bignardi, S., Santarato, G., 2015. A geophysical transect across the central sector of the Ferrara Arc: passive seismic investigations - part II. In: Proceedings of the 34th GNGTS National Convention, vol. 1, pp. 114–120.
Martelli, L., Severi, P., Biavati, G., Rosselli, S., Camassi, R., Ercolani, E., Marcellini, A., Tento, A., Gerosa, D., Albarello, D., Guerrini, F., Lunedei, E., Pileggi, D., Pergalani, F., Compagnoni, M., Fioravante, V., Giretti, D., 2014. Analysis of the local seismic hazard for the stability tests of the main bank of the Po River (Northern Italy). Boll. di Geofis. Teor. Ed. Appl. 55, 119–134.
Mayeda, K., Koyanagi, S., Hoshiba, M., Aki, K., Zeng, Y., 1992. A comparative study of scattering, intrinsic, and coda Q-1 for Hawaii, long valley and central California between 1.5 and 15 Hz. J. Geophys. Res. 97, 6643–6659.
Mucciarelli, M., Gallipoli, M.R., 2001. A critical review of 10 years of microtremor HVSR technique. Boll. di Geofis. Teor. Ed. Appl. 42, 255–266.
Nakamura, Y., 1989. A method for dynamic characteristics estimation of subsurface using microtremor on the ground surface. Q. Report. Railw. Tech. Res. Inst. 30, 25–33.
Nakamura, Y., 1996. Real time information systems for seismic hazards mitigation UrEDAS, HERAS and PIC. Q. Report. Railw. Tech. Res. Inst. 37 (3), 112–127.
Nakamura, Y., 2000. Clear identification of fundamental idea of Nakamura's technique and its applications. In: Proceedings of the 12th World Conference on Earthquake Engineering, New Zealand, 8 pp.
Nogoshi, M., Igarashi, T., 1971. On the amplitude characteristics of microtremor (Part 2). J. Seismol. Soc. Jpn. 24, 26–40 (in Japanese).
Paolucci, E., Albarello, D., D'Amico, S., Lunedei, E., Martelli, L., Mucciarelli, M., Pileggi, D., 2015. A large scale ambient vibration survey in the area damaged by May–June 2012 seismic sequence in Emilia Romagna, Italy. Bull. Earthq. Eng. 13, 3187–3206.
Parolai, S., Bormann, P., Milkereit, C., 2002. New relationships between vs, thickness of the sediments and resonance frequency calculated by means of H/V ratio of seismic noise for the Cologne area (Germany). Bull. Seismol. Soc. Am. 92 (6), 2521–2527.
Pieri, M., Groppi, G., 1981. Subsurface geological structure of the Po Plain, Naples, Italy CNR, Prog. Final. Geodin., Pubbl. no. 414.
Sánchez-Sesma, F.J., Rodríguez, M., Iturrarán-Viveros, U., Luzón, F., Campillo, M., Margerin, L., García-Jerez, A., Suarez, M., Santoyo, M.A., Rodríguez-Castellanos, A., 2011. A theory for microtremor H/V spectral ratio: application for a layered medium. Geophys. J. Int. 186, 221–225. http://dx.doi.org/10.1111/j.1365-246X.2011.05064.x.
RER, ENI-AGIP, 1998. Riserve idriche sotterranee della Regione Emila-Romagna. A cura di G. DI DIO. S.EL.CA. (Firenze).
Scherbaum, F., Hinzen, K.G., Ohrnberger, M., 2003. Determination of shallow shear wave velocity profiles in the Cologne/Germany area using ambient vibrations. Geophys. J. Int. 152, 597–612.
Shiono, K., Ohta, Y., Kudo, K., 1979. Observation of 1–5 s microtremors and their applications to earthquake engineering, Part VI: existence of Rayleigh components. J. Seismol. Soc. Jpn. 35, 115–124.
Tsai, N.C., Housner, G.W., 1970. Calculation of surface motions of a layered half-space. Bull. Seismol. Soc. Am. 60, 1625–1651.